

AD-A050 173

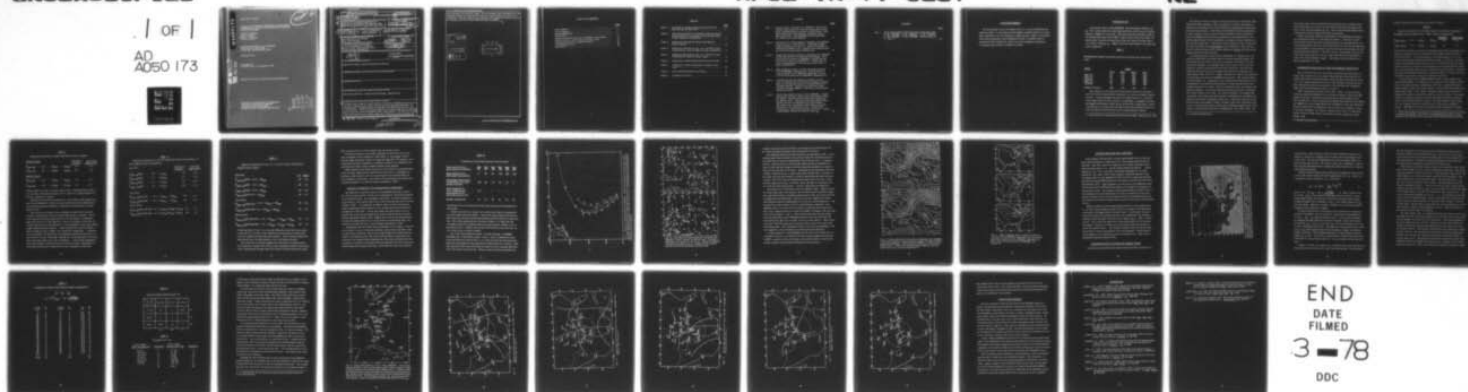
MASSACHUSETTS INST OF TECH CAMBRIDGE DEPT OF METEOROLOGY F/G 4/2
A STUDY OF FORECAST ERRORS IN A BAROTROPIC OPERATIONAL MODEL FO--ETC(U)
DEC 77 F SANDERS, A L ADAMS, N J GORDON F19628-75-C-0059

AFGL-TR-77-0267

NL

UNCLASSIFIED

1 OF 1
AD
A050 173



END
DATE
FILMED
3-78
DDC

AD A050173

AFGL-TR-77-0267

A STUDY OF FORECAST ERRORS IN A BAROTROPIC
OPERATIONAL MODEL FOR PREDICTING PATHS OF
TROPICAL STORMS

Frederick Sanders
Alan L. Adams
Norma J. B. Gordon
Wade D. Jensen

Massachusetts Institute of Technology
Department of Meteorology
Cambridge, Massachusetts 02139

December 1977

Final Report
1 October 1974 - 30 September 1977

Approved for public release; distribution unlimited.

AIR FORCE GEOPHYSICS LABORATORY
AIR FORCE SYSTEMS COMMAND
UNITED STATES AIR FORCE
HANSCOM AFB, MASSACHUSETTS 01731

DDC
RECEIVED
FEB 21 1978
D

AD No. _____
DDC FILE COPY

Unclassified

SECURITY CLASSIFICATION OF THIS PAGE (When Data Entered)

19 REPORT DOCUMENTATION PAGE		READ INSTRUCTIONS BEFORE COMPLETING FORM	
1. REPORT NUMBER (18) AFGL-TR-77-0267	2. GOVT ACCESSION NO.	3. RECIPIENT'S CATALOG NUMBER (9)	
4. TITLE (and Subtitle) (6) A STUDY OF FORECAST ERRORS IN A BAROTROPIC OPERATIONAL MODEL FOR PREDICTING PATHS OF TROPICAL STORMS		5. TYPE OF REPORT & PERIOD COVERED Final Report 1 Oct 1974 - 30 Sept 1977	
6. PERFORMING ORG. REPORT NUMBER		7. CONTRACT OR GRANT NUMBER(s) (15) F19628-75-C-0059	
7. AUTHOR(s) (10) Frederick Sanders, Norma J. B. Gordon Alan L. Adams, Wade D. Jensen		8. CONTRACT OR GRANT NUMBER(s)	
9. PERFORMING ORGANIZATION NAME AND ADDRESS Mass Institute of Technology Dept of Meteorology Cambridge, Massachusetts 02139		10. PROGRAM ELEMENT, PROJECT, TASK AREA & WORK UNIT NUMBERS 62101F (16) 86281201 (17) 12	
11. CONTROLLING OFFICE NAME AND ADDRESS Air Force Geophysics Laboratory Hanscom AFB, Massachusetts 01731 Monitor/Thomas Keegan/LYS		12. REPORT DATE (11) December 1977	
14. MONITORING AGENCY NAME & ADDRESS (if different from Controlling Office) (12) 38p.		13. NUMBER OF PAGES 37	
		15. SECURITY CLASS. (of this report) Unclassified	
		15a. DECLASSIFICATION/DOWNGRADING SCHEDULE	
16. DISTRIBUTION STATEMENT (of this Report) Approved for public release; distribution unlimited.			
17. DISTRIBUTION STATEMENT (of the abstract entered in Block 20, if different from Report)			
18. SUPPLEMENTARY NOTES			
19. KEY WORDS (Continue on reverse side if necessary and identify by block number) Hurricane prediction. Numerical forecasting. Satellite data.			
20. ABSTRACT (Continue on reverse side if necessary and identify by block number) To enable use of satellite cloud-motion vectors in the SANBAR model for prediction of tropical storm tracks, we have derived regression equations for estimating the tropospherically averaged flow from information at one, two, or three levels. Two-level results represent an improvement over climatology and a third level yields substantial further improvement. We find from a study of the 1975 season in the Atlantic Basin that reduction in initial position and track-velocity errors can produce substantial improvement in position-fore-			

DD FORM 1 JAN 73 1473 EDITION OF 1 NOV 65 IS OBSOLETE

Unclassified

SECURITY CLASSIFICATION OF THIS PAGE (When Data Entered)

220 P23

Y/B

cast accuracy out to 72 hours range. We recommend a new procedure for evaluating and using wind observations within the region influenced by the storm circulation. The new method has the potential for substantial reduction of present forecast error for storms within 24 hours of landfall.

ADDITION for	
RTIS	White Section <input checked="" type="checkbox"/>
BDC	Buff Section <input type="checkbox"/>
UNANNOUNCED	<input type="checkbox"/>
JUSTIFICATION.....	
BY.....	
DISTRIBUTION/AVAILABILITY CODES	
Dist.	AVAIL. and/or SPECIAL
A	

DDC
 RECEIVED
 FEB 21 1978
 D

TABLE OF CONTENTS

	<u>Page</u>
List of Tables.....	4
List of Figures.....	5
Acknowledgements.....	7
Introduction.....	8
Regression Estimation of the Tropospheric Mean Wind.....	10
Sources of Error in 1975 Operational forecasts.....	15
Interpretation of Storm Influenced Winds.....	22
Concluding Summary.....	35
References.....	36

TABLES

	<u>Page</u>
Table 1. Homogeneous sample of forecast position errors (nm) over period 1973-1976.....	8
Table 2. Regression equations for estimated zonal and meridional components of tropospherically averaged winds, in NHC region of responsibility.....	11
Table 3. Regression equations for Eastern and Western Pacific regions.....	12
Table 4. Regression equations for one, two, and three levels of information, region of NHC forecast responsibility	13
Table 5. Regression equations for one, two, and three levels of information, Western Pacific region.....	14
Table 6. Comparison of operational and best-track forecasts	16
Table 7. Frequency of values of parameters chosen to minimize V'	26
Table 8. Interrelationship between X_1 and X_3	27
Table 9. Frequency of errors.....	27

FIGURES

	<u>Page</u>
<p>Fig. 1. Tracks of Faye, September 26, 0000GMT. Dashed line indicates observed track, solid line operational forecast track and dotted line best-track revised forecast. Dots show forecast positions, labelled in number of hours after initial time. Corresponding observed positions are shown by hurricane symbols.</p>	17
<p>Fig. 2. Data bases for oceanic analysis, September 26, 0000GMT: a) near surface; b) 200-mb level. Positions of bogus points are shown by circled x's. Radius of influence is shown by the dashed circle. Dashed arrows indicate data not received by operational deadline time.</p>	18
<p>Fig. 3. Large-scale initial flow pattern, September 26, 0000GMT (solid lines) and 48-hr stream-function changes: a) observed and b) predicted by SANBAR. Stream-function lines are at intervals of $3 \times 10^6 \text{ m}^3 \text{ s}^{-2}$. Dashed lines indicate stream-function rises and dotted lines falls, in units of $3 \times 10^6 \text{ m}^3 \text{ s}^{-2}$.</p>	20
<p>Fig. 4. NMC prognostic charts: a) 36-hr barotropic forecast valid at 0000GMT, September 27; b) 24-hr PE baroclinic forecast valid at 0000GMT, September 27; and c) 72-hr PE forecast valid at 0000GMT, September 29.</p>	21
<p>Fig. 5. In shaded area the new analysis procedure is used, while in unshaded area the statistical analysis continues. Open circles indicate location of recently installed rawinsonde stations. Closed circles indicate former stations and bogus points not considered in determining boundary location.</p>	23
<p>Fig. 6. Initial mean winds for July 9, 1959, 0000GMT. Central position and influence region of hurricane symbol Cindy are shown, respectively by the hurricane symbol and the dashed circle. Positions of the storm twelve hours earlier and later are shown by hurricane symbols. The heavy arrow represents a twelve-hour linear displacement at the specified velocity. Plotted winds represent \vec{V}_r, also given by numerical notation. Values in parenthesis denotes the observed wind, \vec{V}_o.</p>	29

FIGURES

Page

- Fig. 7 Initial mean winds for hurricane Delia, September 1973:
a) 4th 1200GMT, b) 5th 0000GMT, c) 5th 1200GMT,
d) 6th 0000GMT, e) 6th 1200GMT. Notation same as
in Fig. 6.

30

ACKNOWLEDGEMENT

We are grateful to Patricia Tayntor, M.I.T., for aid in tabulation and analysis of data, to Roy Jenne and Paul Mulder, National Center for Atmospheric Research, for providing data, to Mark Zimmer, NHC, for providing data and for preparing revised SANBAR forecasts, to Isabelle Kole for preparation of the manuscript, and to Air Force Geophysics Laboratory for support under Contract F19628-75-C-0059.

Table 1

Horizontal range of forecast position errors (km) over period 1973-1974

Model	12 hr	24 hr	48 hr	72 hr
NHC 87	52	117	287	453
NHC 75	53	115	286	386
CLIPER	55	128	283	359
NHC 75	53	115	283	382
SANBAR	56	115	286	376
Number of cases	206	183	133	94

The character of the model was forged by the initial storm minimum. It is the primary physical mechanism for motion of intense tropical storms. Locally speaking, the assertion is that the storm is "steered" by the large-scale winds in which it is embedded, as suggested by Riehl and Howard and Simpson, 1968, and by Jordan, 1972, among others. Hence it seemed that the simple barotropic physics should be examined before any other consideration was devoted to more complex physical effects.

1. From Director's memo on A and B activities at NHC, dated July 16, 1973.

INTRODUCTION

A barotropic filtered model (SANBAR) was developed by Sanders, et. al., 1975, and by others for operational prediction of the tracks of tropical storms at ranges out to 72 hours. This model has been used since 1968 at the National Hurricane Center (NHC), where recent results (see Table 1)¹ indicate that it performs competitively with other objective models which are credited (Dunn et. al., 1968) for the slow improvement in the final subjective judgement.

Table 1

Homogeneous sample of forecast position errors (nm) over period 1973-1976.

<u>Model</u>	<u>Range</u>			
	<u>12 hr</u>	<u>24 hr</u>	<u>48 hr</u>	<u>72 hr</u>
NHC 67	55	117	287	433
NHC 72	53	117	266	386
CLIPER	55	123	268	369
NHC 73	53	113	248	388
SANBAR	56	117	236	348
Number of cases	206	183	135	94

The character of the model was formed by the belief that momentum advection is the primary physical mechanism for motion of intense tropical vortices. Loosely speaking, the assertion is that the storm is "steered" by the larger-scale current in which it is embedded, as suggested by Riehl and Haggard and Sanborn, 1956, and by Jordon 1952, among others. Hence it seemed that the simple barotropic physics should be exploited before serious consideration was devoted to more complex physical effects.

1. From Director's memo on R and D activities at NHC, dated July 15, 1977

The failure of earlier attempts at barotropic prediction (Birchfield, 1960, Vanderman, 1962, Kasahara, 1959, for example) to achieve operational acceptance was regarded as due to the difficulty of establishing an adequate initial large-scale analysis on the basis of rawinsonde-derived pressure data in lower latitudes, where errors are often as large as natural variability. Hence the SANBAR model relies on an analysis of wind observations, averaged through the depth of the troposphere, and makes no direct reference to the pressure-height data. Difficulties with the separation of the vortex from the large-scale flow in the forecasting process (Kasahara, 1959), led us to utilize a relatively small 150-km mesh length and to predict the storm as an integral part of the total flow field.

Two problems had to be dealt with immediately: 1) analysis over the tropical oceans where rawinsonde data are almost completely absent, and 2) assessment of the effect of the storm circulation, as distinct from the large-scale influence, on soundings made in the vicinity of the storm (necessary for realistic construction of the total initial flow). The first was handled by the provision, at first subjectively and later by objective automated means (Pike, 1975),² of "bogus" wind data at a coarse array of points covering large portions of the SANBAR forecast area. The second problem was first handled by subtracting from nearby wind observations a vector contribution from an idealized axi-symmetric vortex specified by the geographical position of its center, and by its maximum wind, eye diameter and radius of influence. All of these parameters except the last are reasonably well known initially in real time. The radius of influence was subjectively determined, with results that often seemed so unsatisfactory that 300nm was adopted as an almost ubiquitous nominal value. When this technique continued to provide unreasonable-looking "residual" large-scale winds from time to time, it was decided to ignore nearby wind soundings altogether and to substitute, at the affected points of the SANBAR grid, first (Pike, 1972), the

2. Private Communication

vector sum of the storm contribution described above and a constant large-scale contribution equal to the recently observed direction and speed of the storm track, and later (Sanders *et. al.*, 1975) a fixed stream-function field calculated from these winds and the storm parameters.

Aside from purely technical improvements in the SANBAR calculations two avenues seem open for improving performance. One stems from the improvement in the large-scale oceanic data base over the past decade, due to increased numbers of better wind observations from aircraft and especially to large numbers of wind estimates now derived from cloud motions observed by geosynchronous satellites. The other road to improvement, however difficult it has been in the past, must lie in the effective use of wind observations in the storm-influenced region. This paper reports principally our efforts along these two lines.

REGRESSION ESTIMATION OF THE TROPOSPHERIC MEAN WIND

The current data base over the oceans comprises relatively dense coverage in the lowest 2 km, from surface observations by ship and from low cloud-motion observations by satellite, and in the layer from 9 km to 12 km, from wind observations derived from aircraft navigation systems and from high cloud-motions observed by satellite. We must infer the tropospheric mean wind from information in these two layers.

Thus, following preliminary work by Pike (1975)¹, we derived some definitive regression equations from an extensive sample of data in the NHC region of forecast responsibility during the period June through October, 1971 through 1974. In these equations rawinsonde wind observations at 850mb and 250mb were used to approximate the tropospheric mean wind calculated from the winds at the ten mandatory pressure levels from 1000mb to 100mb in the same soundings. Our results, obtained from a total of 11,682 observations in June through October at Bermuda, San Juan, Hatteras, Miami, Tampa, Lake

1. Private communication

Charles, Brownsville and Merida, are given in Table 2.

Table 2

Regression equations for estimated zonal and meridional components of tropospherically averaged winds, in NHC region of responsibility.

			<u>reduction of variance</u>	<u>root-mean square error</u>
$\hat{u}_{1000-100mb}$	$= +0.4 + .53u_{850} + .37u_{250}$.92	3.4
$\hat{v}_{1000-100mb}$	$= -0.5 + .45v_{850} + .33v_{250}$.85	3.1

Note that the reduction of variance is substantial and that the meridional component is somewhat less well represented (presumably because of noisier vertical structure). Note further that the root-mean square error, if not reduced by the analysis and initialization processes, is sufficient to produce nearly all the present state-of-the-art error in a 24-hour forecast by simple constant steering, even aside from additional error introduced by use of data other than rawinsonde observations in equations tailored for them. Evidently the value of the equations would be to reduce the large error in the occasional dreadful forecast made in near-total ignorance far at sea.

In the anticipation that SANBAR might be used in other regions of the Northern Hemisphere, we obtained similar equations for the Eastern Pacific (from 5,594 observations at Vandenberg AFB, Hilo, Johnston Island and Midway Island). and for the Western Pacific (from 10,145 observations from Guam, Wake Island, Truk, Ponape, Kwajalein, Majure, Yap, and Koror).¹ Equations for these two additional regions are given in Table 3. The results indicate no substantial difference between the Atlantic and Eastern Pacific areas. In the Western Pacific, however, the zonal equation is quite different, and it appears that the vertical structure of the zonal component is noisier. Although the reduction of variance in both components is smaller

1. The former of these sets may not represent the wind structure in the zone of tropical cyclogenesis, where next to no rawinsonde data exist, but they should be more reliable as the storm approaches these populated locations.

Table 3

Regression equations for Eastern and Western Pacific regions.

<u>Eastern Pacific</u>				<u>reduction of variance</u>	<u>root-mean- square error</u>
$\hat{u}_{1000-100}$	=	+0.2	+ .52u ₈₅₀ + .36u ₂₅₀	.87	3.9
$\hat{v}_{1000-100}$	=	+0.1	+ .46v ₈₅₀ + .36v ₂₅₀	.88	3.3
 <u>Western Pacific</u>					
$\hat{u}_{1000-100}$	=	-2.2	+ .43u ₈₅₀ + .32u ₂₅₀	.77	3.3
$\hat{v}_{1000-100}$	=	-0.4	+ .40v ₈₅₀ + .26v ₂₅₀	.70	2.7

in this region, so is the root-mean-square error, indicating that the wind is less variable in the Pacific sample, but we cannot tell to what extent the reduction is temporal or spatial.

Stratification of the above samples into early-season (June-August) and late-season (September-October) portions showed only minor differences in the resulting regression equations, reductions of variance and root-mean-square errors.

The accuracy of estimate of the tropospheric-mean wind is, however, sensitive to the number of levels at which information is available. We derived regression equations appropriate for the unfortunate circumstances when only low-level or only high-level data were available, and for the optimistic hope that wind information for a mid-tropospheric level (say, 500mb) might somehow become available. These equations are shown in Tables 4 and 5 in which the data of Table 1 are included for comparison. If only one level is available, the mean wind can probably be specified with little or no skill relative to local climatology, although one is somewhat better off to have data in the upper than in the lower troposphere. If the middle tropospheric data could be added to observations at the other two levels, substantial improvement would be felt in specification of the tropospheric mean wind.

Table 4

Regression equations for one, two, and three levels of information, region of NHC forecast responsibility.

One level:				<u>reduction of variance</u>	<u>root-mean square error</u>
$\hat{u}_{1000-100}^{(850)}$	=	+4.8	+ .71 u_{850}	.43	8.8
$\hat{u}_{1000-100}^{(250)}$	=	-2.1	+ .43 u_{250}	.69	6.5
$\hat{v}_{1000-100}^{(850)}$	=	-1.5	+ .51 v_{850}	.34	6.6
$\hat{v}_{1000-100}^{(250)}$	=	0.9	+ .35 v_{250}	.60	5.2
Two levels:					
$\hat{u}_{1000-100}^{(850, 250)}$	=	+0.4	+ .53 u_{850} + .37 u_{250}	.92	3.4
$\hat{v}_{1000-100}^{(850-250)}$	=	-0.5	+ .45 u_{850} + .33 u_{250}	.85	3.2
Three levels:					
$\hat{u}_{1000-100}^{(850, 500, 250)}$	=	-0.1	+ .31 u_{850} + .36 u_{500} + .26 u_{250}	.97	1.9
$\hat{v}_{1000-100}^{(850, 500, 250)}$	=	-0.3	+ .30 v_{850} + .35 v_{500} + .24 v_{250}	.95	1.8

Table 5

Regression equations for one, two, and three levels of information ,
Western Pacific region.

		RV	RMSE
One level:			
$\hat{u}_{1000-100}^{(850)} = -4.5 + .28u_{850}$.24	6.0
$\hat{u}_{1000-100}^{(250)} = -5.9 + .22u_{250}$.28	5.8
$\hat{v}_{1000-100}^{(850)} = -0.8 + .40v_{850}$.24	4.3
$\hat{v}_{1000-100}^{(250)} = 0.2 + .26v_{850}$.42	3.7
Two levels:			
$\hat{u}_{1000-100}^{(1000, 250)} = -2.2 + .43u_{850} + .32u_{250}$.77	3.3
$\hat{v}_{1000-100}^{(1000, 250)} = -0.4 + .40v_{850} + .26v_{250}$.70	2.7
Three levels:			
$\hat{u}_{1000-100}^{(850, 500, 250)} = -0.8 + .28u_{850} + .3.2u_{500} + .25u_{250}$.92	1.9
$\hat{v}_{1000-100}^{(850, 500, 250)} = -0.4 + .30v_{850} + .31v_{500} + .24v_{250}$.89	1.7

Comparing Tables 4 and 5, we see large differences when data are available at only one level, because of the different vertical structure of wind fields in the two regions; but when data are available at three levels the regression equations and the root-mean-square errors, are almost identical.

The reductions of variance suggest more skill than is actually present in the equations, because part of the variance doubtless resides in differences in the climatological average wind from station to station within each region.

This is particularly true of the sample from the Atlantic sector,

We made no attempt to use zonal components as predictors for meridional components of the tropospheric mean winds, or vice versa. Such an attempt might yield useful results if trough and ridge tilts, for example, were consistently northeast-southwest or northwest-southeast, but substantial improvement over what we have already obtained seems unlikely.

When satellite cloud-motion vectors are used in place of rawinsonde data in the two-level-equations (as would be done in practice, for example) we estimate a 50% increase in the root-mean-square error of specification of the tropospheric-mean wind. The details of this estimation, and of the entire regression analysis, are given by Adams and Sanders (1975).

SOURCES OF ERROR IN 1975 OPERATIONAL FORECASTS

We undertook to study the causes of large SANBAR forecast errors in the 1975 hurricane season, with the aim of applying our regression equations in revised predictions. As a preamble to this effort, we made revised forecasts based on post-season "best-track" initial positions and track velocities (Hebert, 1976). As illustrated in Table 6, these revised forecasts presented a substantial improvement over the original operational predictions at ranges out to 48 hours. On the other hand, the mean initial errors in position and track velocity (based on the premise that the best-track information represents absolute truth), suggest that it will be extremely difficult to reduce the mean position error in the 24-hour forecast below 75nm, the expected (or hoped-for) error cited by Sanders and Burpee, (1968).

Incidentally, the 1975 tracks were remarkable in two respects: only one storm failed to recurve toward the northeast, and no storm executed a loop or other exotic excursion. There was a slight tendency for operational positions to lie westward of the best-track locations and for operational track velocities to be insufficiently northeastward, both biases probably due to the forecasters' reluctance to anticipate fully the degree of recurvature and acceleration which was actually occurring. In the event of erratic storm tracks,

Table 6.

Comparison of operational and best-track forecasts

Mean position error, operational forecasts(nm)	00hr 15	12hr 67	24hr 121	36hr 181	48hr 261	72hr 393
Mean position error, best-track forecasts(nm)	0	50	99	152	224	376
Percentage improvement of best-track over oper- ational forecasts.	100	25	18	16	14	4
Mean magnitude of error in operational specification of ini- tial track velocity (kts)	2.8	-	-	-	-	-
Number of forecasts	74	67	58	51	44	33

operational errors in initial position and track velocity would probably have been larger.

Twenty forecasts were chosen for revision on the basis of reanalysis of the initial large-scale flow pattern. These were about equally split between those that were particularly good operationally and those that were especially bad. (Were only egregiously poor forecasts chosen, it is likely that any reasonable alteration of method would show improvement, whether or not it had general merit.) Sanders and Gordon (1976) found the large forecast errors to stem from a variety of causes.

One of the cases analyzed in detail, for Faye starting at 0000GMT, September 26, is illustrated in Figs. 1 and 2. From a comparison of predicted and observed tracks in Fig. 1, it is seen first that the slow predicted speed was responsible for the large 212-nm operational error at 24 hr, which was improved in the best-track prediction only by a more accurate specification of the initial track direction. Second, neither forecast anticipated the

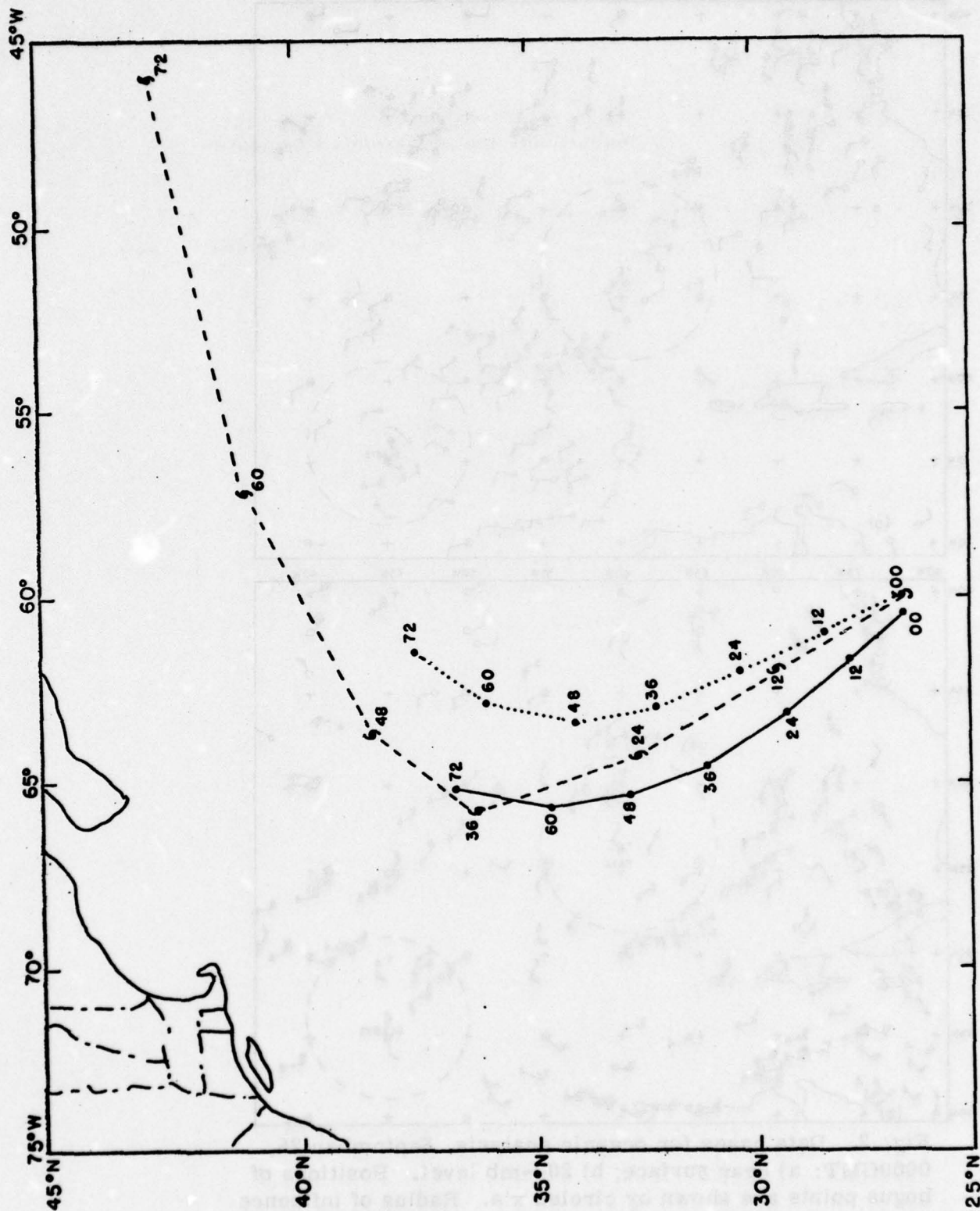


Fig. 1. Tracks of Faye, September 26, 0000 GMT. Dashed line indicates observed track, solid line operational forecast track, and dotted line best-track revised forecast. Dots show forecast positions, labelled in number of hours after initial time. Corresponding observed positions are shown by hurricane symbols.

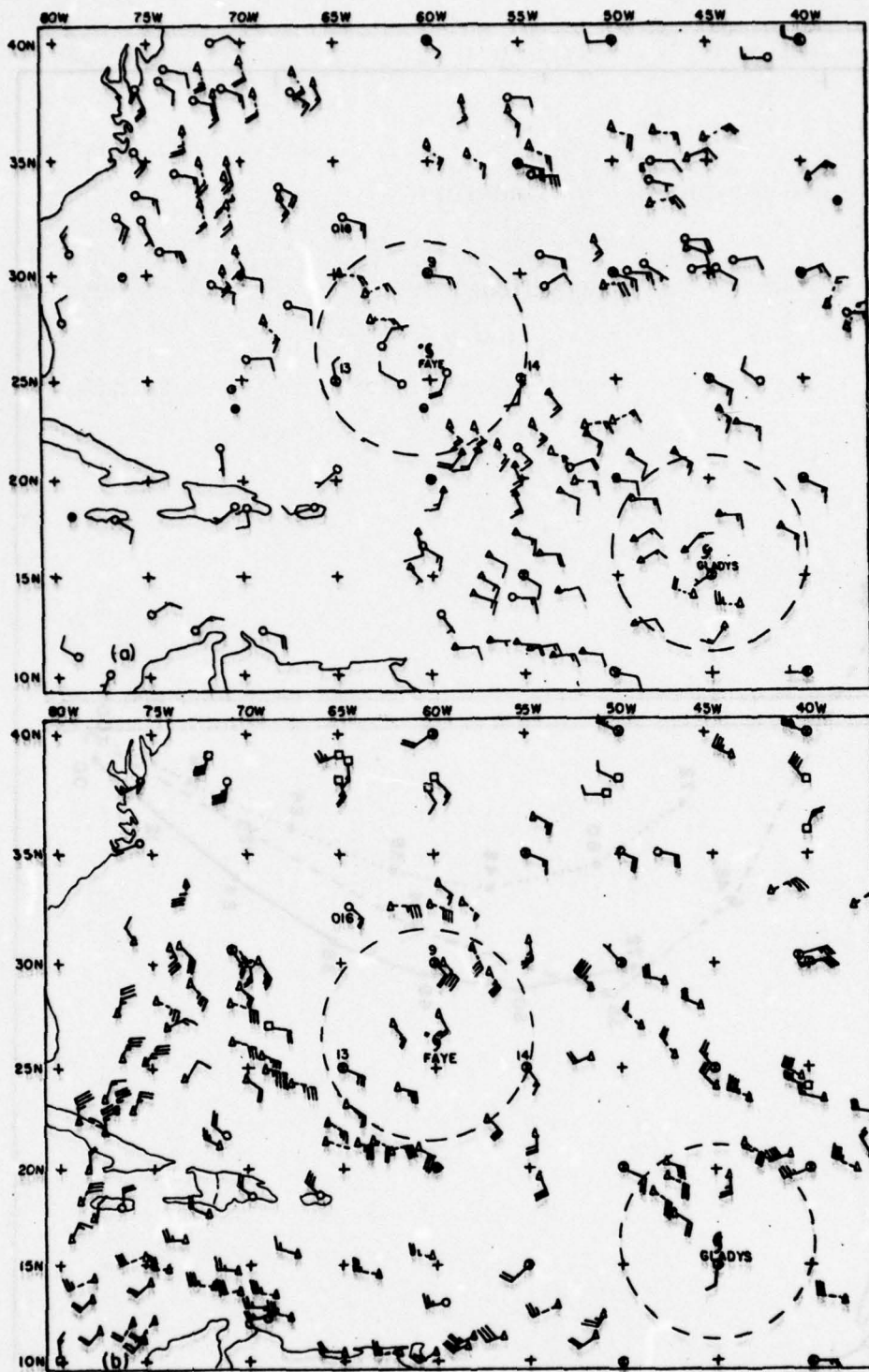


Fig. 2. Data bases for oceanic analysis, September 26, 0000GMT: a) near surface; b) 200-mb level. Positions of bogus points are shown by circled x's. Radius of influence is shown by the dashed circle. Dashed arrows indicate data not received by operational deadline time.

dramatic acceleration after 48 hours, producing errors of 961 nm and 772 nm in the operational and best-track predictions at 72 hours.

The unusually dense initial observational coverage shown in Fig. 2, comprising mainly wind estimates from satellite-observed cloudmotion vectors, precludes lack of data as an explanation of the forecast errors. It appears, however, that the numerous observations within the 300-nm influence distance of Faye indicate a large-scale flow toward the northwest at a speed in excess of the specified initial speed. Application of the regression equations in Table 1 indicate in fact, a large-scale speed of about 15kt, in contrast to the initial 11kt specified initially in both the operational and best-track predictions. The 12-hr observed displacement speed was in fact 17kt. In the present analysis procedure, of course, these wind data are discarded in favor of the specified initial speed. Clearly, useful data are being lost.

The large error at 72 hours arises from another cause. Figure 3 shows the initial large-scale flow pattern, with its observed and predicted change. The ridge which initially extended northwestward of the storm was predicted to change little during 48 hours, whereas in fact the trough in the central United States advanced northeastward to pick up the accelerating storm. The forecast error was evidently not due to fixed boundary conditions in the SANBAR model, but rather to the presence of important baroclinic effects. This view is supported by the portions of the NMC hemispheric 500-mb prognostic charts shown in Fig. 4. Note that the barotropic forecast suffers from the same defect as the SANBAR prognosis, while the baroclinic PE forecast has the right idea, as usual, but is a bit slow about it. Note further from Fig. 2 that the large-scale structure in the vicinity of the storm was hardly barotropic. The tropospheric shear in this case was substantial and well organized, with a probable direct effect upon storm behavior.

In other instances, large SANBAR forecast errors were found to be attributable to failure to use satellite-derived pressure-height data poleward of 30°N , to paucity of data of all types, and to fixed values of vorticity and stream function on the northern boundaries of the grid area.

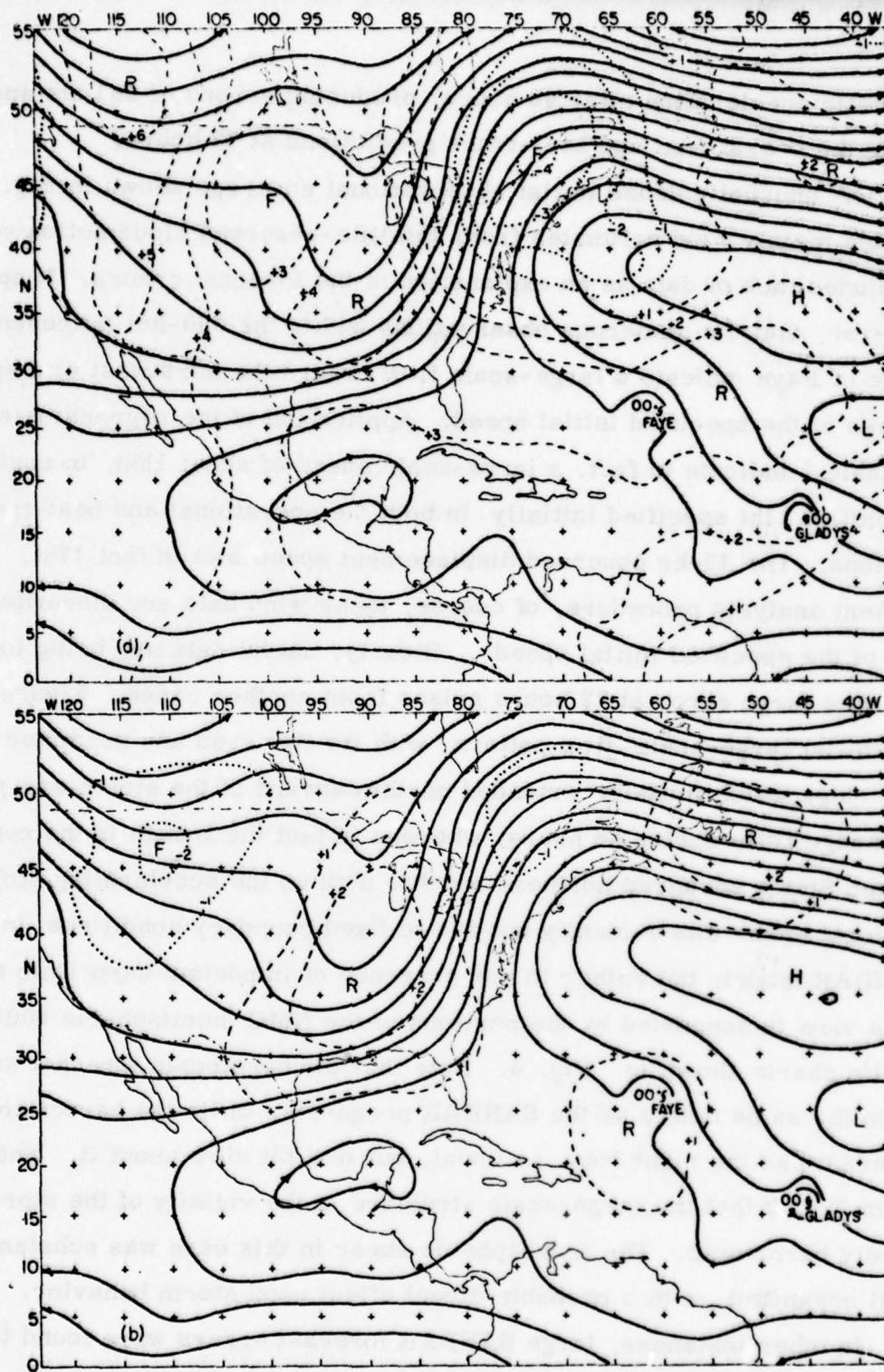


Fig. 3. Large-scale initial flow pattern, September 26, 0000GMT (solid lines) and 48-hr stream-function changes: a) observed and b) predicted by SANBAR. Stream-function lines are at intervals of $3 \times 10^6 \text{ m}^3 \text{ s}^{-2}$. Dashed lines indicate stream-function rises and dotted lines falls, in units of $3 \times 10^6 \text{ m}^3 \text{ s}^{-2}$.

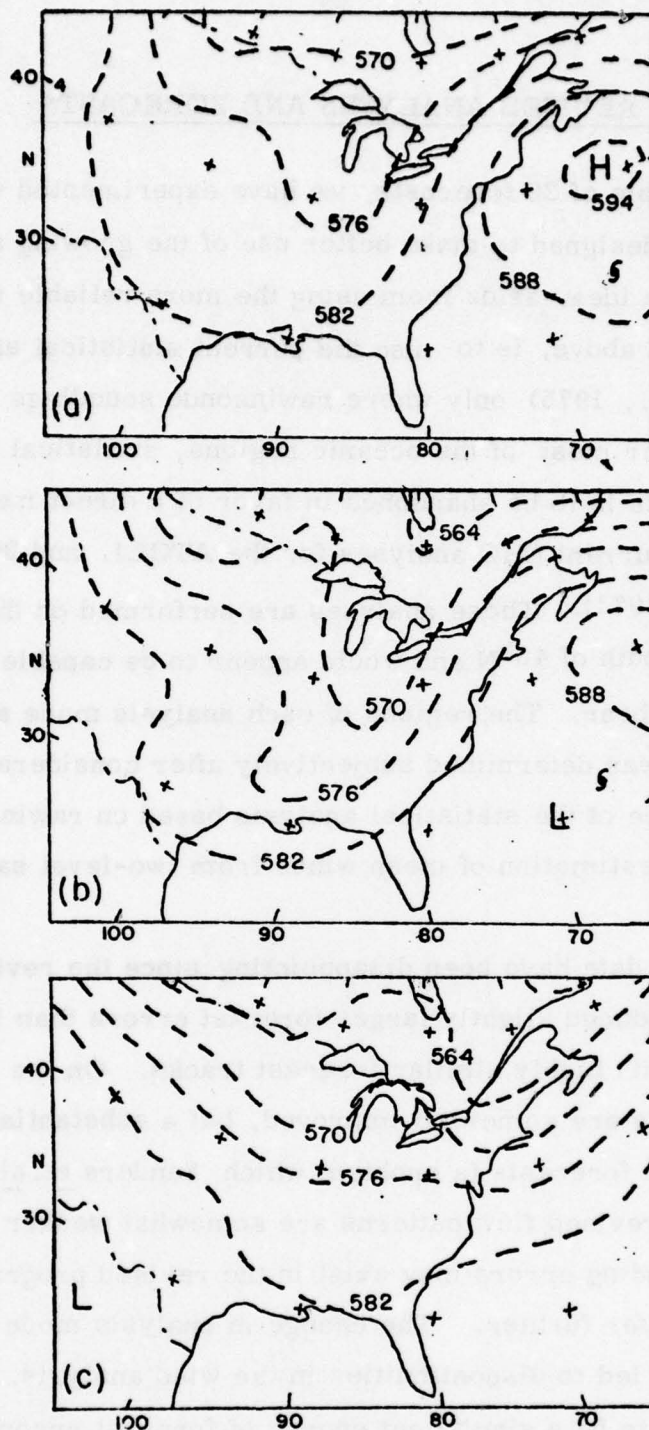


Fig. 4. NMC prognostic charts: a) 36-hr barotropic forecast valid at 0000GMT, September 27; b) 24-hr PE baroclinic forecast valid at 0000GMT, September 27; and c) 72-hr PE baroclinic forecast valid at 0000GMT, September 29.

REVISED ANALYSES AND FORECASTS

In the sample of 20 forecasts, we have experimented with a revised analysis method designed to make better use of the growing satellite-derived data base. The idea, aside from using the more reliable regression equations discussed above, is to use the current statistical analysis method (Sanders *et. al.*, 1975) only where rawinsonde soundings are available. Elsewhere, over most of the oceanic regions, statistical analysis via the few bogus points is to be abandoned in favor of a direct mean-wind analysis derived from current NHC analyses for the ATOLL and 200-mb levels (Wise and Simpson, 1971). These analyses are performed on the SANBAR computational grid south of 45°N and would appear to be capable of bringing more information to bear. The regions of each analysis made are shown in Fig. 5. The boundary was determined subjectively after consideration of the unexplained variance of the statistical analysis based on rawinsonde data and the uncertainty of estimation of mean winds from two-level satellite cloud-motion vectors.

Results to date have been disappointing, since the revised analysis procedure has produced slightly larger forecast errors than in the operational predictions, with highly similar forecast tracks. On the whole, forecast track directions are somewhat improved, but a substantial slow bias has reappeared in the forecasts (a problem which Sanders *et. al.*, 1976, deemed solved). The revised flow patterns are somewhat weaker over the oceans. We suspect coding errors may exist in the revised program and intend to pursue the matter further. The change in analysis mode across the boundaries in Fig. 5 led to discontinuities in the wind analysis. These however, did not appear to be a significant source of forecast error. This work is discussed in detail by Gordon (1977).

INTERPRETATION OF STORM INFLUENCED WINDS

It seems that rawinsonde observations made within the circulation of a

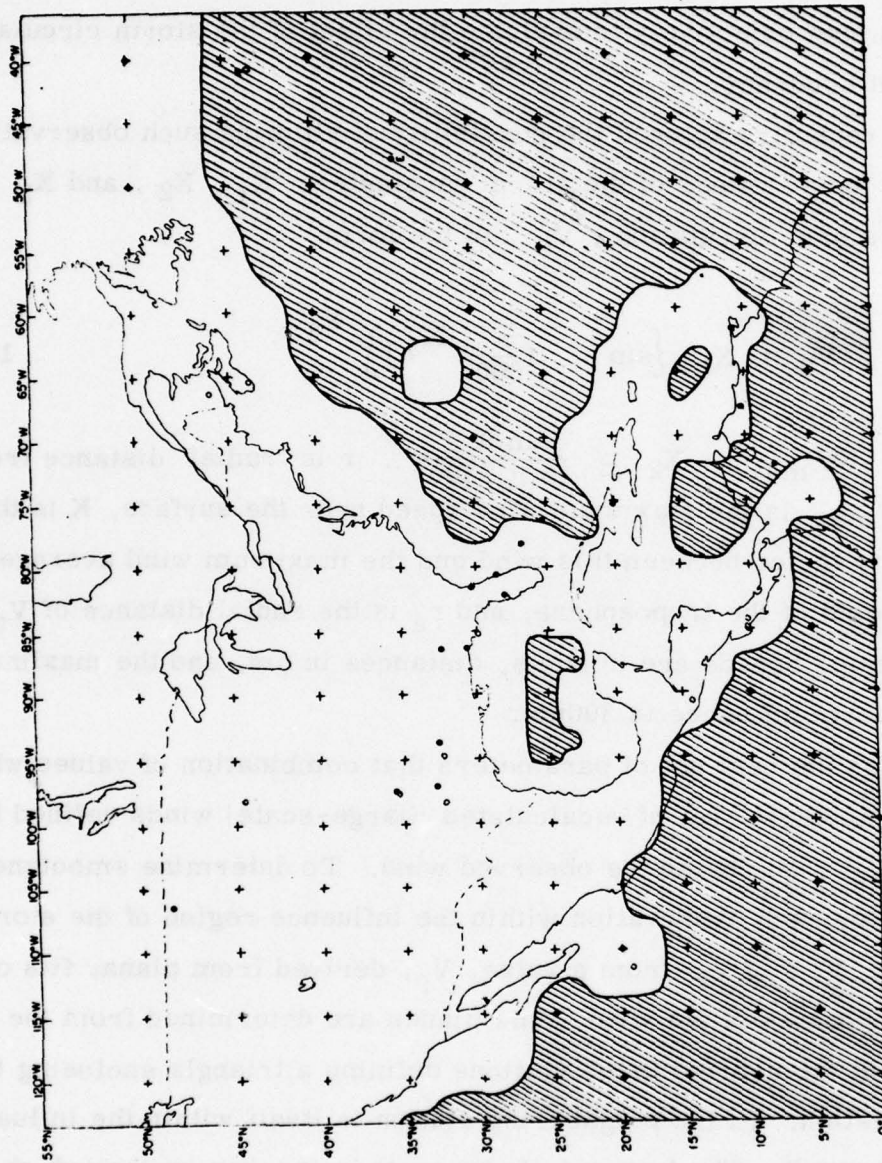


Fig. 5. In shaded area the new analysis procedure is used, while in unshaded area the statistical analysis continues. Open circles indicate location of recently installed rawinsonde stations. Closed circles indicate former stations and bogus points not considered in determining boundary location.

tropical storm, often with great difficulty and at substantial hazard to the observers, should be a valuable source of information concerning the track of the storm. Yet both the SANBAR and the Hovermale MFM (1975), discard all such observations. The reason, in the case of SANBAR, is that we have not been able objectively to evaluate the effect of the storm circulation with sufficient accuracy.

We have recently explored the possibility of allowing such observations to tell us the "best" values of the storm parameters X_1 , X_2 , and X_3 for a symmetric storm circulation, V_θ , of the form

$$V_\theta = X_1 \left\{ \sin \left[\left(\frac{r}{300} \right)^{X_2} \right] \right\}^{X_3} \quad 1)$$

where $X_1 \equiv KV_{\max}$, $X_2 \equiv \frac{\ln 0.5}{\ln(r_e/300)}$, r is radial distance from the center, V_{\max} is the maximum wind speed near the surface, K is the proportionality factor between this wind and the maximum wind averaged through the depth of the troposphere, and r_e is the radial distance of V_{\max} from the center. Speeds are in knots, distances in nm, and the maximum distance of storm influence is 300nm.

We take as the best set of parameters that combination of values which yields the "smoothest" set of recalculated (large-scale) winds defined by $V_r \equiv V_o - V_\theta$, V_o being the observed wind. To determine smoothness, we calculate for each observation within the influence region of the storm, the deviation, V' , of V_r from a value, V_p , derived from planar fits of the u - and v -components of the wind. The planes are determined from the values of V_o or V_r at the nearest three stations defining a triangle enclosing the station in question. (If the neighboring station is itself within the influence region, V_r is used). The best set of parameters is taken as that which minimizes the root-mean-square value of V' over all stations for each synoptic case.

Finally, of course, the values of V_r should provide a good specification of the storm-track velocity at the time of the observations. We would hope

that this specification is as accurate as the operational estimate made in real time by NHC for the official advisories. To this end, a value of \bar{V}_r at the location of the storm center was determined, for the optimum set of storm parameters, by stepwise screening regression for both zonal and meridional wind components, given the station values of \bar{V}_r .

Fifty data sets, for nine tropical storms, were chosen for study on the basis of the presence of two or more simultaneous rawinsonde observations within the influence region of the storm. Understandably, these storms lay within 300nm or so of the United States coast and thus represented especially important forecast problems for NHC. The parameters, X_1 , X_2 , and X_3 were given discrete sets of values, with resulting selection frequencies as shown in Table 7. We note with surprise that in about half the instances the implied value of V_{\max} is no more than 35kt, and that the shape of the radial profile is very flat, as evidenced by small values of X_3 . The current operational SANBAR value of $X_3 = 1.5$ is exceeded less than 20% of the time in the present sample. Study of individual cases shows that the tropical storm is often embedded in a relatively weak cyclonic circulation of large scale, and that really strong winds are rarely sampled by the rawinsonde system, leading to these unexpected results. Table 8 confirms an association of small values of X_1 and X_3 .

For each synoptic case, we compared the specified initial track velocity emerging from the regression analysis with an estimate of the actual initial velocity obtained from the best-track information. The mean magnitude of the vector difference was 4.2 knots, slightly worse than the probable discrepancy between operationally-specified and best-track initial velocities, as discussed earlier. The frequency distribution of the differences in Table 9 shows, however, that operational accuracy was probably exceeded about half the time, and that our regression procedure occasionally yielded extremely large errors. Examination of cases showed that these tended to be instances in which rawinsonde observations were available in only a single quadrant of the storm. There was little bias in specified direction or speed.

Table 7

Frequency of values of parameters chosen to minimize V'

$$\underline{V}' = \underline{V}_r - \underline{V}_p$$

$$x_1 = 0.72V_{\max} ; x_2 = \frac{\ln 0.5}{\ln (r_e/300)}$$

<u>x_1(kt)</u>	<u>N</u>	<u>r_e(nm)</u>	<u>N</u>	<u>x_3</u>	<u>N</u>
5	0	3	7	0.2	13
10	8	6	1	0.4	5
15	6	9	5	0.6	3
20	7	12	4	0.8	6
25	4	15	7	1.0	2
30	1	18	1	1.2	6
35	4	21	2	1.4	5
40	2	24	2	1.6	2
45	3	27	2	1.8	2
50	0	30	2	2.0	1
55	0	33	2	2.2	0
60	0	36	1	2.4	0
65	1	39	2	2.6	1
70	2	42	1	2.8	0
75	3	45	1	3.0	2
80	0	48	2	3.2	1
85	2	51	1	3.4	0
90	5	54	1	3.6	0
95	2	57	1	3.8	0
100	0	60	5	4.0	1
Total	50		50		50

Table 8

Interrelationship between X_1 and X_3

$X_1 \backslash X_3$	0.2-0.6	0.8-1.8	2.0-4.0	
5 - 20	17	4	none	21
25-45	4	9	1	14
65-95	none	10	5	15
	21	23	6	

Table 9

Frequency of errors

Error range: Track velocity (kts)	Frequency	Error range: Position error (nm)	Frequency
(0-1.7)	7	0 - 20	5
(1.8-3.3)	9	21 -40	11
(3.4-5.0)	14	41-60	16
(5.1-6.7)	11	61-80	8
(6.8-8.3)	4	81-100	3
(8.4-10)	3	101-120	3
(> 10)	2	120 →	4
	<u>50</u>	Total	<u>50</u>

A deficiency in westward motion might be expected due to our neglect of the effects of the latitudinal variation of earth vorticity, but the effect is evidently small enough to be masked by other sources of error.

In a few cases in which the storm center was very close to a sounding location the regression result was extremely sensitive to the position of the center and large errors were likely. Ten cases of this type were recalculated with the station less than 85nm of the center excluded, yielding much improved results. Figure 6 shows such a case, in which the error is 13 knots. If the storm center were located 17nm to the northnortheast, however, and the storm wind contribution to the Charleston observation were increased from 22 to 28 kts, then a perfect specification would have resulted. Modest asymmetry in the storm circulation as well as moderate position error could produce the large specification error.¹ Thus, we are still unable to make constructive use of observations very close to the storm center.

An especially interesting storm is Delia 1973, which performed a loop along the Texas Gulf Coast before moving inland. The operational SANBAR 24-hour forecasts were very poor during this time, for obvious reasons. The numerous observations within the influence region were discarded in favor of a straight uniform large-scale flow representing the most recent storm-track vector. Our new procedure, as illustrated in Fig. 7, shows excellent specification of the track velocity during the loop (probably better than the velocity estimated in real time), as Delia and a larger-cyclone, denoted by the heavy block letter, circle about each other. The looping motion of Delia seems plainly accountable as a barotropic process. The motion of the larger cyclone is a moot question.

Although the new procedure has not been incorporated in the SANBAR analysis program, we estimated the errors that would have ensued from using the specified track velocity as a 12-hour extrapolation forecast. The average position error was 55 nm, the same as the 12-hour errors shown in Table 1,

1. A recalculation with the Charleston observations excluded yielded an error of three knots.

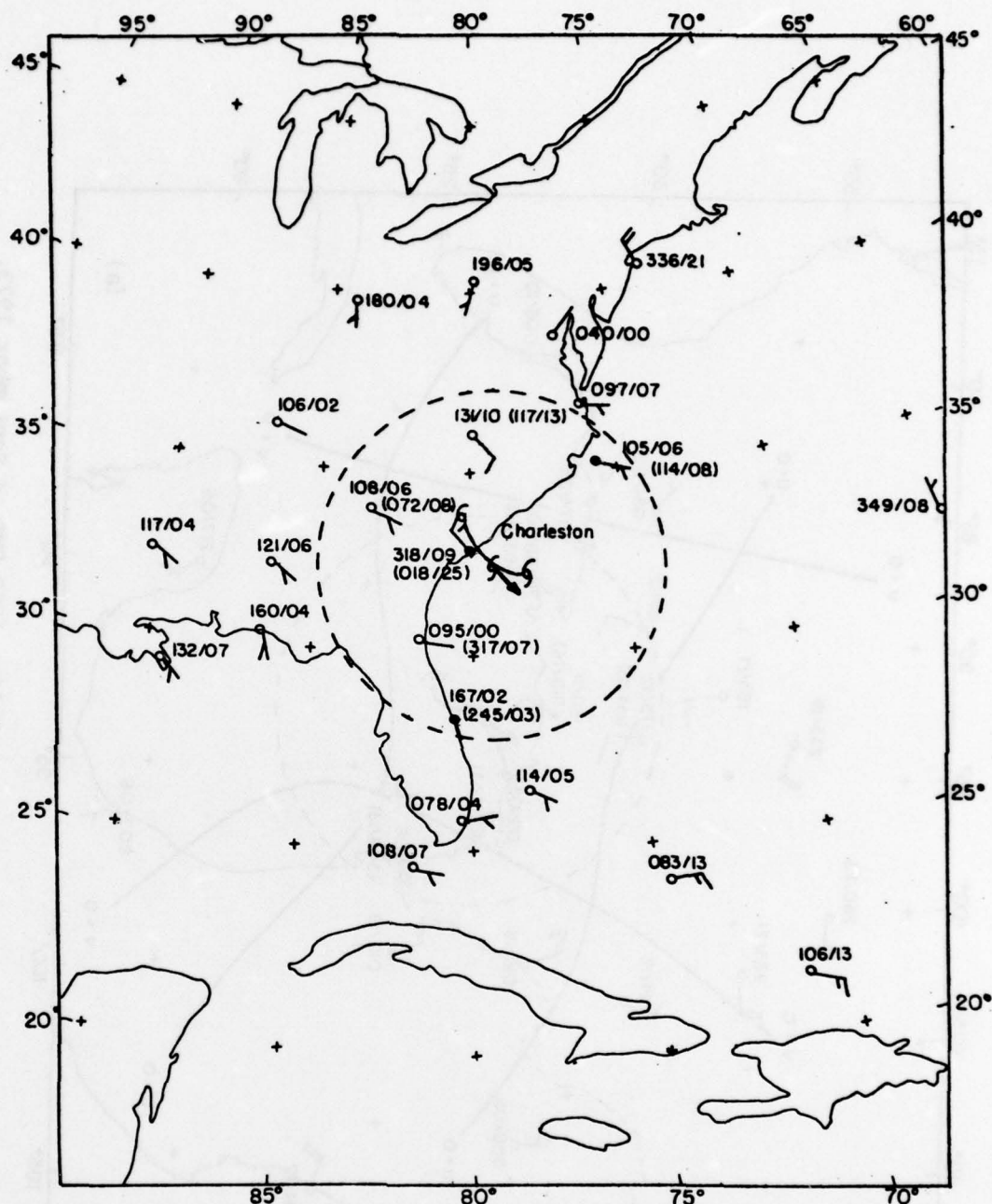


Fig. 6. Initial mean winds for July 9, 1959, 0000GMT. Central position and influence region of hurricane symbol Cindy are shown, respectively by the hurricane symbol and the dashed circle. Positions of the storm twelve hours earlier and later are shown by hurricane symbols. The heavy arrow represents a twelve-hour linear displacement at the specified velocity. Plotted winds represent \underline{V}_r , also given by numerical notation. Values in parenthesis denotes the observed wind, \underline{V}_o .

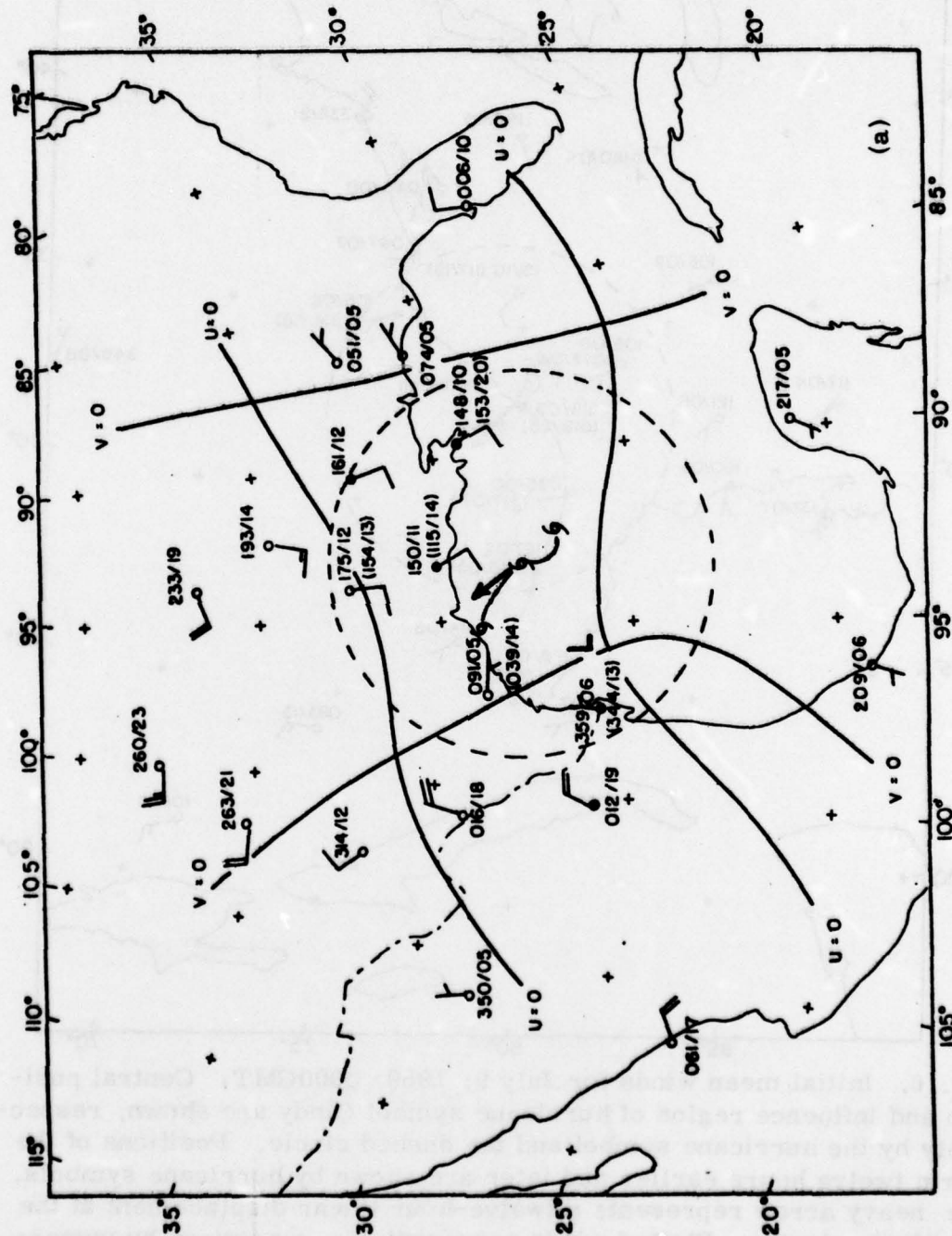


Fig. 7a Initial mean winds for hurricane Delia, 1200 GMT, 4 September 1973.
Notation same as in Fig. 6.

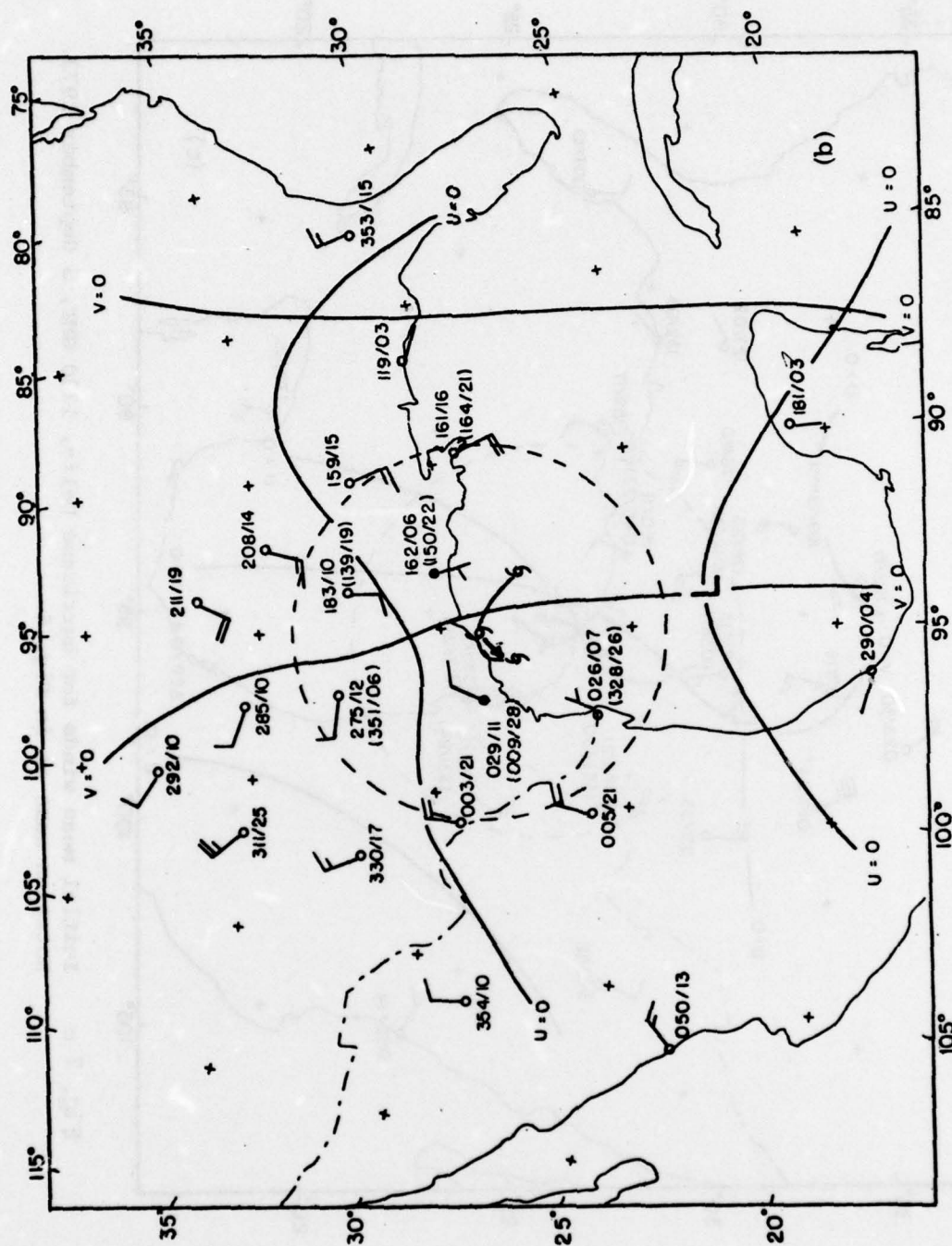


Fig. 7b Initial mean winds for hurricane Delia, 0000GMT, 5 September 1973.
Notation same as in Fig. 6.

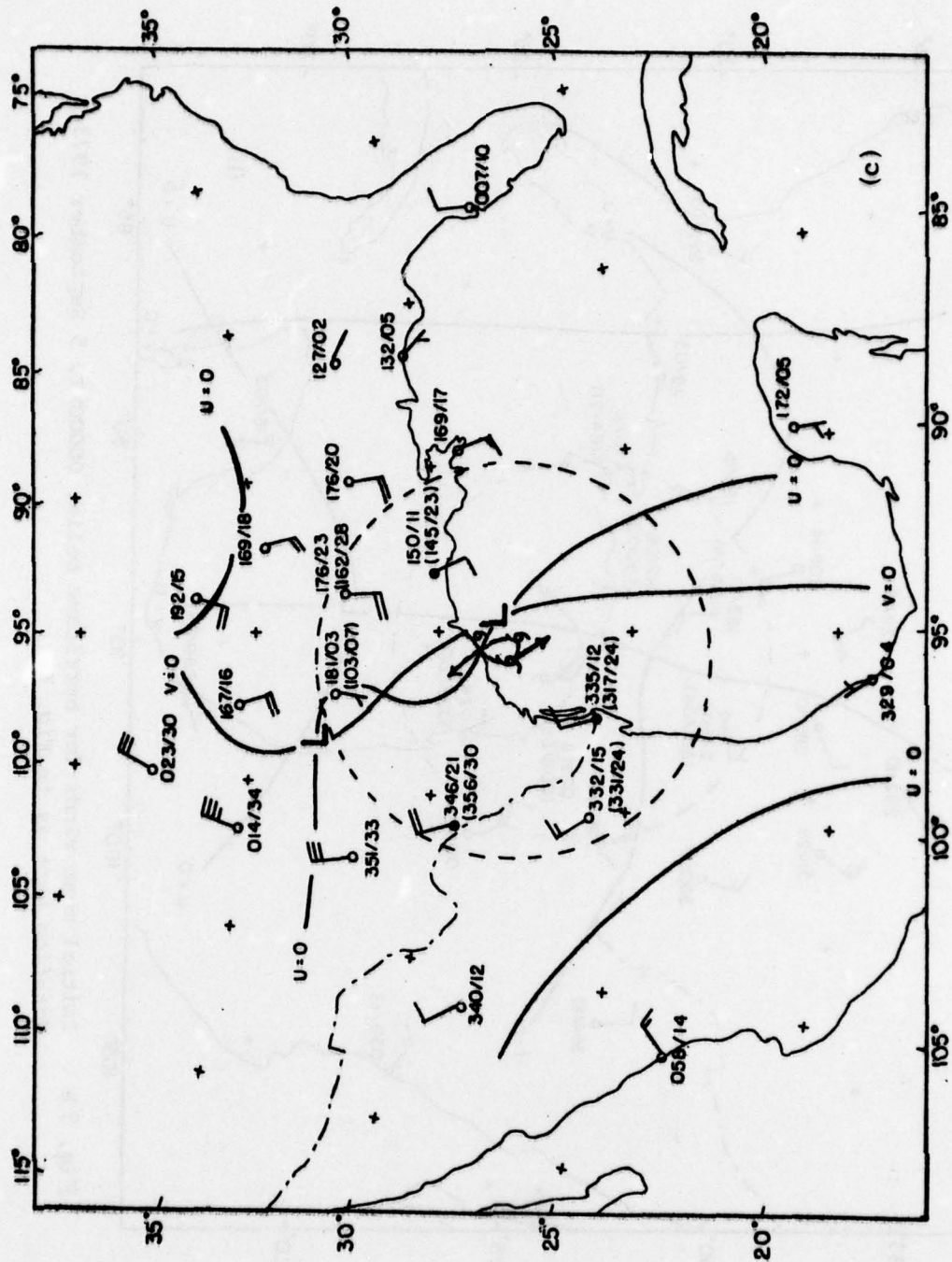


Fig. 7 c Initial mean winds for hurricane Delia, 1200 GMT, 5 September 1973.
Notation same as in Fig. 6.

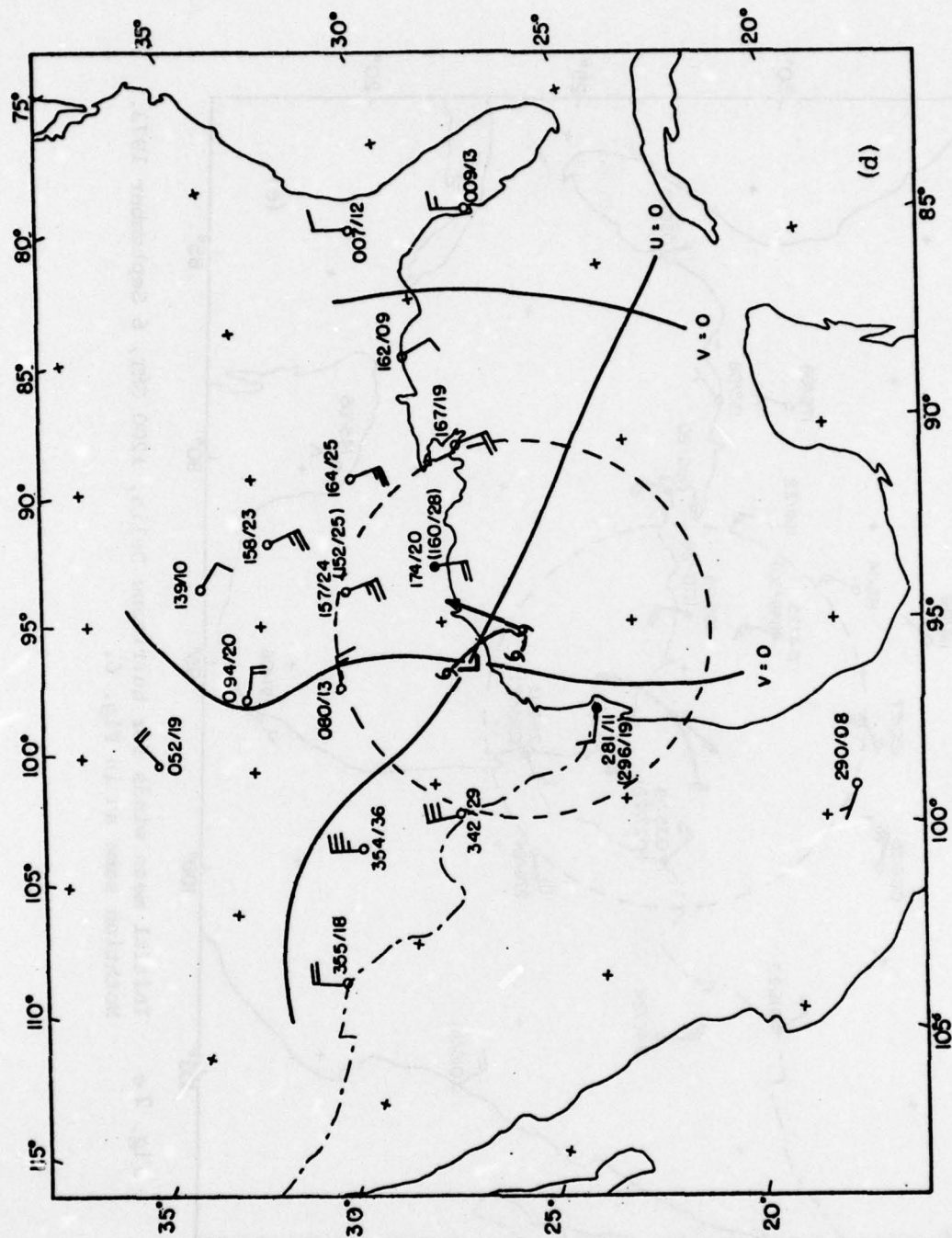


Fig. 7 d Initial mean winds for hurricane Delia, 0000GMT, 6 September 1973.
Notation same as in Fig. 6.

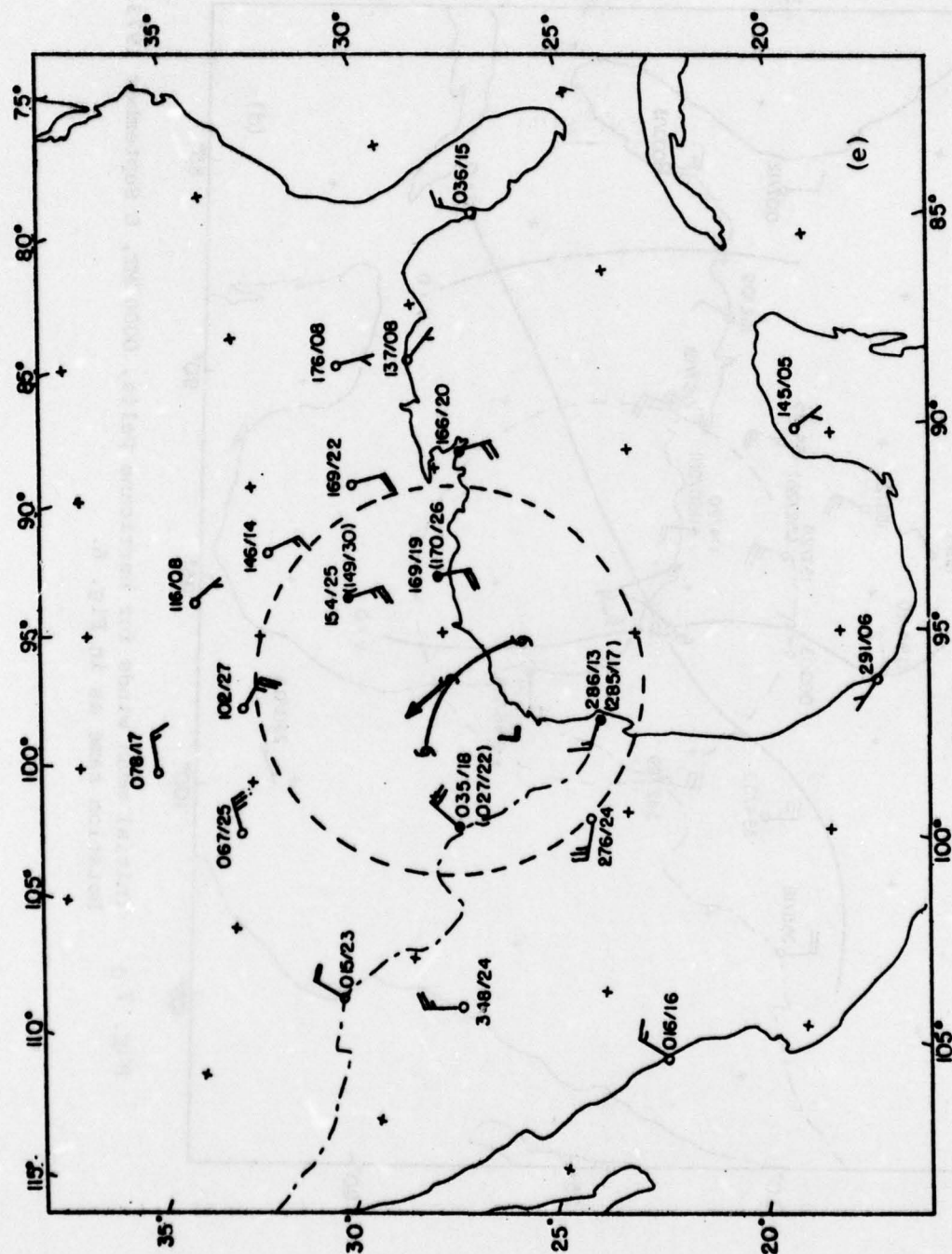


Fig. 7 e Initial mean winds for hurricane Delia, 1200 GMT, 6 September 1973.
Notation same as in Fig. 6.

but probably better than current capability in seasons with more erratic tracks than 1973 to 1976. This limitation aside, primary potential advantage of the new procedure is that the large-scale flow in the storm-influenced region is not constrained to be uniform.

CONCLUDING SUMMARY

For use of satellite cloud-motion vectors in the SANBAR prediction model, we have derived some definitive regression formulas, for the zonal and meridional components of the wind averaged over the depth of the tropical troposphere, given data in the lower or upper troposphere alone, in both these layers, and in the middle troposphere as well as in these layers. We find that data at only one level yield a result little better than use of the climatological mean, while addition of middle-tropospheric data, difficult with current satellite capability, would improve substantially upon estimates based on lower-and upper-tropospheric data. We find some benefit in use of separate formulas for the Atlantic and Pacific areas, but little in stratification into earlier and later portions of the tropical-storm season.

From a study of SANBAR forecast errors, we find that the present model suffers from inadequate use of observations within the storm-influenced region, from neglect of pressure-height data outside the tropics, from fixed boundary conditions in the middle-latitude portion of the forecast grid, and from neglect of baroclinic effects in the large-scale flow pattern surrounding the storm.

We recommend a new procedure for use when three or more rawinsonde observations lie within the storm-influenced region. This procedure, in which the observations determine some parameters of the storm circulation itself, appears capable of specifying the initial storm-track velocity about as well as present subjective practice, but removes the present SANBAR assumption of a uniform large-scale flow within the storm-influenced region. It should be especially useful when erratic tracks occur close to landfall.

REFERENCES

- Adams, A. L., and F. Sanders, 1975: Application of satellite cloud-motion vectors to hurricane track prediction, Sci. Rep. No. 1 Contract F 19628-75-C-0059 AFCRL-TR-75-0635.
- Birchfield, G. E., 1960: Numerical prediction of hurricane movement with the use of a fine grid, J. Meteor., 17, 406-414.
- Dunn, G. E., R. C. Gentry, and B. M. Lewis, 1968: An eight-year experiment in improving forecasts of hurricane motion, Mon. Wea. Rev., 96, 708-713.
- Gordon, N. J. B., 1977: A revised procedure for analysis of initial data for a dynamical hurricane track prediction model. SM thesis, Mass. Inst. of Technology, Cambridge.
- Hebert, P. J., 1976: Atlantic hurricane season of 1975, Mon. Wea. Rev., 104, 453-465.
- Hovermale, J. B., 1975: First season storm movement characteristics of the NMC objective hurricane forecast model. Paper presented at Twelfth Annual NOAA NWS Warning Service Evaluation Conference, Coral Gables, Florida.
- Jordan, E. S., 1952: An observational study of the upper-wind circulation around tropical storms, J. Meteor. 9, 340-346.
- Kasahara, A., 1959: A comparison between geostrophic and nongeostrophic numerical forecasts of hurricane movement with the barotropic steering model, J. Meteor., 16, 371-384.
- Pike, A. C. 1972: Improved barotropic hurricane track prediction by adjustment of the initial wind field. NOAA Tech. Memo. NWS SR-66
- Riehl, H., W. H. Haggard, and R. W. Sanborn: On the prediction of 24-hour hurricane motion, J. Meteor., 13, 415-420.
- Sanders, F., and R. W. Burpee, 1968: Experiments in barotropic hurricane track forecasting, J. Appl. Meteor., 7, 313-323.
- Sanders, F., A. C. Pike, and J. P. Gaertner, 1975: A barotropic model for operational prediction of tracks of tropical storms. J. Appl. Meteor., 14, 265-280.

Sanders, F., and N.J. Gordon, 1976: A study of forecast errors in an operational model for predicting paths of tropical storms, Sci. Rep. No. 2, Contract F19628-75-C-0059 AFGL-TR-77-0079.

Vanderman, L.W. 1962: An improved NWP model for forecasting the paths of tropical cyclones, Mon. Wea. Rev., 90, 19-22.

Wise, C.W., and R.H. Simpson, 1971: The tropical analysis program on the National Hurricane Center. Weatherwise, 24, 164-173.